Spanwise scale selection in plane mixing layers

By MICHAEL M. ROGERS AND ROBERT D. MOSER
NASA-Ames Research Center, Moffett Field, CA 94035, USA

(Received 6 March 1992 and in revised form 3 September 1992)

Direct numerical simulations of temporally evolving plane mixing layers undergoing as many as three pairings have been examined for evidence of spanwise scale change. All simulations were begun from a few low-wavenumber disturbances, usually derived from linear stability theory, in addition to the mean velocity. The amplitude of the initial three-dimensional disturbances varied from infinitesimal to large enough to trigger a rapid transition to turbulence. The time required for a change of characteristic spanwise scale with infinitesimal three-dimensional disturbances was found to be very long, requiring three or more pairings to complete a doubling of the spanwise scale. Stronger three-dimensionality can produce more rapid scale changes, but it is also likely to trigger transition to turbulence. No evidence was found for a change from an organized array of rib vortices at one spanwise scale to a similar array at a larger spanwise scale.

1. Introduction

Flow visualizations in several experiments done in the 1970s indicated that a predominantly streamwise secondary structure existed in the braid regions of plane mixing layers (Miksad 1972; Brown & Roshko 1974; Konrad 1976; Breidenthal 1981). This structure was investigated further by others and found to consist of streamwise vortices, which were nearly aligned with the strain field of the predominantly two-dimensional spanwise rollers (Bernal 1981; Jimenez, Cogollas & Bernal 1985; Bernal & Roshko 1986; Lasheras, Cho & Maxworthy 1986).

Lin & Corcos (1984) showed that streamwise vorticity present in the braid regions of a plane mixing layer will 'collapse' into compact vortices if the circulation associated with the streamwise vorticity is large enough compared to its characteristic spanwise scale, the strain rate due to the spanwise rollers, and the viscosity of the fluid. Streamwise vortices become apparent in flow visualization experiments when their vorticity collapses.

The spanwise scale of the streamwise vortices is highly variable. Stability calculations by Pierrehumbert & Widnall (1982) show that the most amplified spanwise wavelength associated with a periodic array of Stuart (1967) vortices is about two-thirds of the fundamental disturbance wavelength, but that disturbances with considerably longer and shorter wavelengths have nearly the same growth rate. Corcos & Lin (1984) confirmed this insensitivity to spanwise scale for the more realistic case of an evolving two-dimensional base flow. The experiments of Lasheras & Choi (1988) found no appreciable difference in growth rate for disturbances between one-fifth and three times the fundamental wavelength in their experiments using serrated splitter-plate trailing edges. Nygaard & Glezer (1991) were able to generate streamwise vortices with virtually any spanwise wavelength using their splitter-plate heater mosaic. Despite this broad range of possible spanwise

wavelengths, many 'naturally evolving' mixing layers seem to have a characteristic spanwise scale that is close to that predicted by Pierrehumbert & Widnall (1982).

There is, however, a considerable difference of opinion regarding changes in spanwise scale that may occur as a result of the streamwise scale changes during pairings. Flow visualizations by Bernal & Roshko (1986) indicate that their rib spacing remains constant through several pairings, until the completion of the so-called 'mixing transition'. Recent experiments by Bell & Mehta (1992) indicate a spanwise scale change at the location of the second pairing according to the criterion for pairing locations proposed by Huang & Ho (1990). Bell & Mehta (personal communication) feel that this location may actually correspond to the third pairing. On the other hand, a three-dimensional reconstruction of a pairing event by Jimenez *et al.* (1985) indicates that the number of streamwise vortices is halved after a pairing. Jimenez (1983) postulated a mechanism for this scale change, in which neighbouring ribs annihilate each other, leaving ribs at twice the original spanwise scale but with the same circulation as before. Similarly Huang & Ho (1990) find that the preferred spanwise scale doubles after both the first and second pairings in their experiments, and suggest that it would continue to double with each pairing. Experiments to date thus seem to indicate that the locations of spanwise scale changes may be facility dependent.

Here we address the issue of spanwise scale change using numerical simulation. In particular, the conditions under which a scale change occurs and the mechanisms for such a scale change are investigated. Numerical simulation is ideally suited to this task since it allows precise specification of disturbances and provides a detailed description of the flow field. In previous work by Moser & Rogers (1993, hereafter referred to as MR), and Rogers & Moser (1992), a thorough examination of rib vortices, and three-dimensionality in general, was undertaken for numerically simulated mixing layers undergoing up to three pairings of the spanwise rollers. These flows are re-examined for evidence of spanwise scale change, and new simulations designed to elucidate possible spanwise scale change mechanisms are studied as well.

As in MR, the direct numerical simulations examined here are of the time-developing mixing layer and were generated by the pseudospectral numerical method outlined in Spalart, Moser & Rogers (1991). The use of simple 'clean' initial conditions allows a controlled study of spanwise scale changes. The governing equations, non-dimensionalization used, description of the initial conditions, and definitions of many quantities (e.g. Fourier-mode amplitudes $A_{\alpha\beta}$) examined in this paper are given in §2 of MR, which immediately precedes this paper in the Journal.

The evolution of infinitesimal three-dimensional disturbances is described in §2, while that of finite-amplitude initial disturbances is given in §3. A brief summary and discussion can be found in §4.

2. Scale change of infinitesimal three-dimensional disturbances

Linear stability analysis of the inviscid Stuart (1967) vortices (Pierrehumbert & Widnall 1982) suggests that there is a most unstable spanwise wavelength for three-dimensional disturbances that is proportional to the roller spacing. One might therefore suppose that the most unstable wavelength would increase with pairings, providing a linear mechanism for a change in spanwise lengthscale. To determine if such a linear mechanism exists, the evolution of infinitesimal three-dimensional perturbations with $\frac{1}{8} \leqslant \beta \leqslant 4$ is considered in mixing layers that undergo as many as

Simulation	A_{1_0} $\times 10^2$	$A_{\frac{1}{2}0}$ $\times 10^2$	$A_{\frac{1}{4}0}$ $\times 10^2$	$A_{\frac{1}{8}0}$ $\times 10^2$	τ_r	τ_{o0}	τ_{p1}	τ_{s1}	τ_{o1}	τ_{p2}	τ_{s2}	τ_{o2}	τ_{p3}	τ_{s3}
2D0P	4.00	—	—	—	13.4	17.5	—	—	—	—	—	—	—	—
2D1P	4.00	3.00	—	—	11.9	—	21.5	29.2	46.5	—	—	—	—	—
2D2P	4.00	3.00	3.00	—	11.9	—	21.5	31.2	—	46.7	63.9	90.3	—	—
2D3P	4.00	3.00	3.00	3.00	11.9	—	21.5	32.0	—	47.0	66.7	—	103.7	139.8

TABLE 1. Parameters of the two-dimensional simulations. Disturbance profiles are eigenfunctions, $Re_0 = 250$, $\phi_{\alpha 0} = 0$, and $\lambda_x = 1.16(2\pi)$ for all cases. 2D3P was not run long enough to determine τ_{o3}.

three pairings (β is a scaled spanwise wavenumber, see MR for definition). These computations have also been used to find the wavelength of the initially fastest growing disturbance, thereby determining the value of the fundamental spanwise disturbance wavelength λ_z used here and in Rogers & Moser (1992) and MR.

Three-dimensional disturbances with various spanwise wavelengths have been allowed to evolve in four different two-dimensional base flows, which undergo zero, one, two, or three pairings (2D0P, 2D1P, 2D2P, and 2D3P, respectively). Initial conditions and the times at which several important events occur (see MR) are given for each base flow in table 1. The times include the rollup time τ_r (When A_{1_0} reaches its first maximum), the pairing times τ_{pn} (where the nth pairing time is given by the first maximum of $A_{\frac{1}{2^n}0}$), the spiral-arm re-entry times τ_{sn}, and the oversaturation times τ_{on}, where the subscript n indicates association with the nth pairing. As noted in MR, the spiral-arm re-entry time is the time at which the spiral arms of spanwise vorticity created after a pairing are advected into the mid-braid plane. This occurs after each pairing and thus each pairing has an associated spiral-arm re-entry. After the flow pairs for the last time (or if it does not pair fast enough) it eventually 'oversaturates', with spanwise vorticity re-entering the mid-braid region and remaining their continuously (see MR). This occurs only after the last pairing in each of these base flows. The four base flows and the significance of the times defined above (along with their definitions) are discussed in detail in MR.

The amplitude evolution of disturbances with various spanwise wavelengths is shown in figure 1 for each of the four base flows. For the single-pairing base flow (2D1P, figure 1*b*) disturbances with $\frac{1}{4} \leqslant \beta \leqslant 4$ are considered. Over most of the time period shown, the largest amplitude is attained by the $\beta = 1$ disturbance. For this reason, the spanwise wavelength $\lambda_z = 0.6\lambda_x$ was chosen as the fundamental ($\beta = 1$) wavelength in Rogers & Moser (1992), MR, and this paper.

For the remaining three base flows, only disturbances with $\beta < 1$ are considered because the most unstable spanwise wavelength should increase as the characteristic streamwise scale (the roller spacing) increases by pairing. Indeed the wavelength of the disturbance with the largest amplitude does increase in the two- and three-pairing cases (figure 1*c*, *d*). However, this change in the dominant scale occurs slowly. For example, the dominant scale does not double even after two pairings in the two- and three-pairing flows (figure 1*c*, *d*). After the third pairing, the amplitude of the first subharmonic exceeds that of the fundamental but not that of the $\beta = \frac{3}{4}$ disturbance (figure 1*d*). However, the growth rate of the subharmonic disturbance ($\beta = \frac{1}{2}$) is about 15% larger than that of the $\beta = \frac{3}{4}$ disturbance by the end of the three-pairing simulation (2D3P) and therefore it appears that $A^*_{s\frac{1}{2}}$ will eventually overtake $A^*_{s\frac{3}{4}}$, although this doubling of the dominant spanwise scale may not occur until a fourth pairing has occurred. Thus linear analysis does not support a 'self-similar'

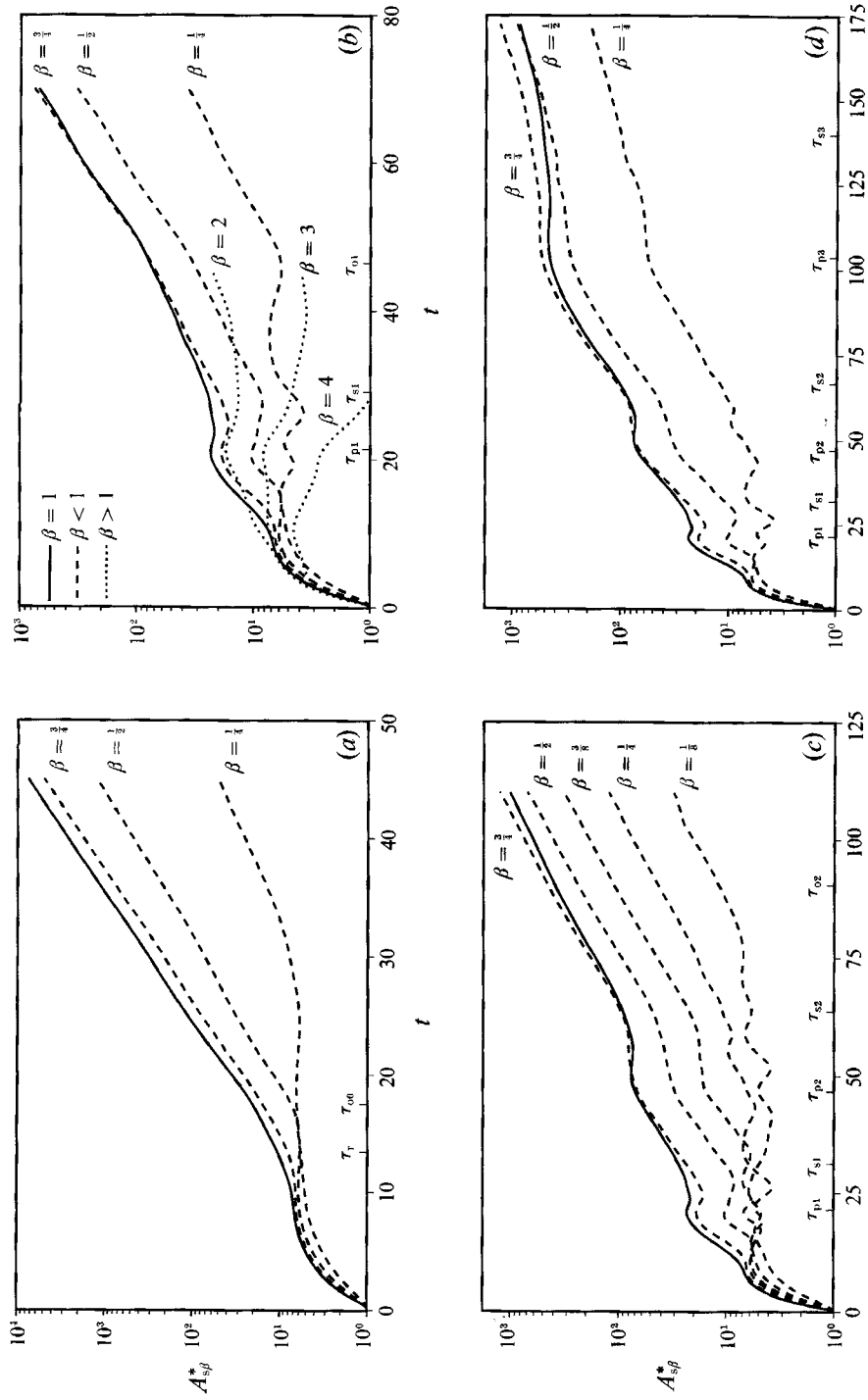

FIGURE 1. Time development of three-dimensional disturbance amplitudes ($A^*_{s\beta}$) of various spanwise wavelength disturbances for (*a*) 2D0P, (*b*) 2D1P, (*c*) 2D2P, and (*d*) 2D3P.

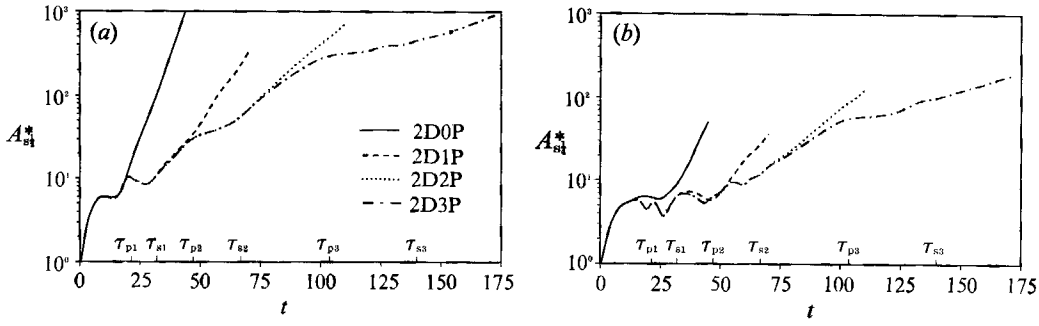

FIGURE 2. Time development of (*a*) $A^*_{s\frac{1}{2}}$ and (*b*) $A^*_{s\frac{1}{4}}$ for disturbances evolving in each of the two-dimensional base flows.

picture of mixing-layer growth, where each pairing is accompanied by a doubling of the characteristic spanwise lengthscale.

The evolution of $A^*_{s\frac{1}{2}}$ and $A^*_{s\frac{1}{4}}$ is replotted in figure 2 (that of A^*_{s1} is given in figure 5 of MR) to facilitate comparison among the base flows. As was found in MR, the evolution for each base flow departs from that of base flows that undergo further pairings at oversaturation.

Disturbances with wavelengths several times larger than λ_z are largely stable until (well) after oversaturation. As can be seen in figure 1, disturbances with $\beta = \frac{1}{4}$ and $\frac{1}{8}$ do not grow for a long period (after the initial increase in amplitude associated with the buildup of ω_y for $t < 10$, see §3.1 of Rogers & Moser 1992). The $\beta = \frac{1}{4}$ disturbances finally begin to grow after the second pairing (τ_{p2}) in the two- and three-pairing cases (figure 2*b*). There is apparently a low-wavenumber cutoff for disturbance growth prior to oversaturation, which is between $\beta = \frac{1}{2}$ and $\frac{1}{4}$ until the second pairing and then shifts to $\frac{1}{8} < \beta < \frac{1}{4}$. As with the dominant scale, the cutoff wavelength does not appear to double with each pairing.

After oversaturation, all the perturbations with $\beta \leqslant 1$ eventually begin to grow. The $\beta = \frac{1}{4}$ disturbances begin to grow after τ_{o1} in 2D1P and well after τ_{o0} in 2D0P. Similarly, the $\beta = \frac{1}{8}$ disturbance begins growing after τ_{o2} in 2D2P. As can be seen in figure 1, after oversaturation the disturbances have similar growth rates, with the longest-wavelength perturbations growing somewhat slower. It was demonstrated in Rogers & Moser (1992) and MR that it is only after oversaturation that the translative instability of Pierrehumbert & Widnall (1982) is active, and Pierrehumbert & Widnall showed that this instability is insensitive to the spanwise wavelength. The above observations indicate that the pre-oversaturation growth of disturbances is more wavelength selective than that associated with the translative instability.

A possible explanation for the slow change in the dominant and cutoff spanwise wavelengths may be found by examining the structure of the two-dimensional base flow (see §3 of MR). For large Reynolds number, the diameter of the region of concentrated spanwise vorticity in the roller core increases by a factor of $\sqrt{2}$ with each pairing, rather than by a factor of 2. If the cutoff and dominant wavelengths increase with the diameter of the roller core vorticity concentration, the wavelength would only grow as the square root of the spacing between the rollers. In Rogers & Moser (1992), it was shown that the analysis of Waleffe (1990) could be used to predict the growth rate and most unstable wavelength of the three-dimensional disturbance in a rolled up mixing layer. This analysis also suggests that the dominant spanwise wavelength should indeed be proportional to the size of the vorticity

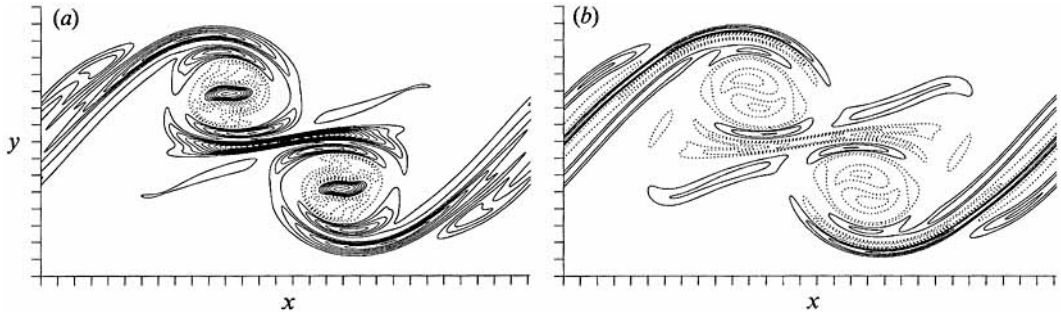

FIGURE 3. Contours of ω_x in the rib plane (RP) for perturbations with (*a*) $\beta = 1$ and (*b*) $\beta = \frac{1}{8}$ at $t = 40.4$ ($\tau_{p2} = 46.7$) on a base flow undergoing two pairings (2D2P). The contour increments are (*a*) $3\Gamma_x^0/(\delta_\omega^0)^2$ and (*b*) $0.04\Gamma_x^0/(\delta_\omega^0)^2$. In this and subsequent similar figures solid contours indicate positive vorticity, dotted contours indicate negative vorticity and tic marks are at δ_ω^0 intervals.

concentration in the roller core. These arguments suggest that the wavelength of the fastest growing perturbation and the cutoff wavelength should double with every two pairings. The data presented here are consistent with this speculation, although they are too limited to confirm it.

The structure of the perturbation vorticity field associated with the largely stable wide-spanwise-wavelength disturbances differs from that of the fundamental ($\beta = 1$) disturbances. As an example, streamwise vorticity contours for both $\beta = 1$ and $\frac{1}{8}$ disturbances are shown in figure 3 at a time shortly before the second pairing. In addition to being much weaker, the ω_x structure in the $\beta = \frac{1}{8}$ case is qualitatively different; for example, the engulfed rib vorticity is negative rather than strongly positive and the braid region contains layers of ω_x that alternate in sign.

3. Nonlinear scale change

In the preceding section it was found that the linear mechanism by which the dominant spanwise wavelength changes was very slow. However, this apparently contradicts the (nonlinear) experimental results of Huang & Ho (1990), which suggest that the dominant spanwise scale should double after each pairing. In this section, nonlinear mechanisms that could hasten a scale change are investigated. The initial condition parameters for the flows used here are given in table 2. Note that the flows PH01P, PH$\frac{1}{8}\pi$1P and PH$\frac{1}{4}\pi$1P are identical except for the relative phasing of the three-dimensional disturbances (the value of $\phi_{0\frac{1}{2}}$ is 0, $\frac{1}{8}\pi$, and $\frac{1}{4}\pi$, respectively). Also PH$\frac{1}{4}\pi$0P is identical to PH$\frac{1}{4}\pi$1P except for the lack of a pairing.

While the phase of the fundamental streamwise invariant disturbance, ϕ_{01}, is irrelevant to the flow evolution (it is set to zero for convenience), the subharmonic phases *are* important. The range over which the subharmonic phase $\phi_{0\frac{1}{2}}$ (MR, equation (9)) can be varied without including redundant cases is from 0 to $\frac{1}{4}\pi$. If there are no other subharmonics, initial conditions with $\phi_{0\frac{1}{2}}$ equal to either endpoint of this range will have one of two spatial symmetries, which are preserved by the Navier–Stokes equations. For $\phi_{0\frac{1}{2}} = 0$ the z-plane-reflection symmetry given by equation (10) in MR is satisfied, with symmetry planes as given in §2.3 of MR. When $\phi_{0\frac{1}{2}} = \frac{1}{4}\pi$ the point-reflection symmetry in equation (11) of MR holds, with symmetry points as given in §2.3 of MR. When a second subharmonic is added ($(0, \frac{1}{4})$ mode), the range of non-redundant phases $\phi_{0\frac{1}{4}}$ is from 0 to $\frac{1}{2}\pi$ is $\phi_{0\frac{1}{2}} = 0$, from $\frac{3}{8}\pi$ to $\frac{7}{8}\pi$ if $\phi_{0\frac{1}{2}} = \frac{1}{4}\pi$, and from 0 to π otherwise. When $\phi_{0\frac{1}{2}}$ is 0 or $\frac{1}{4}\pi$ and $\phi_{0\frac{1}{4}}$ equals one of the

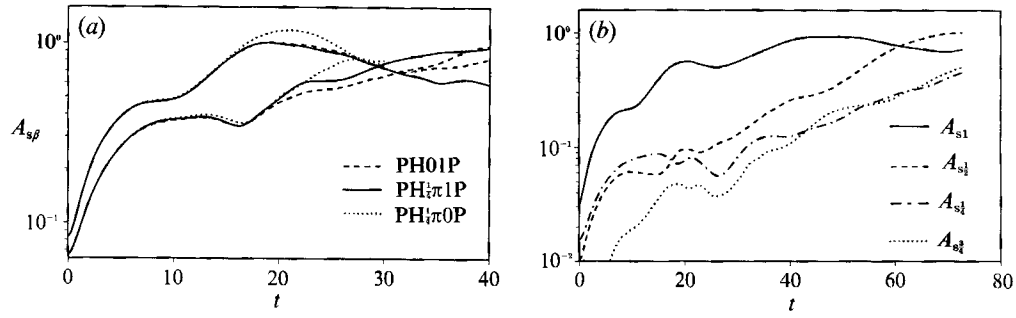

FIGURE 4. Time development of three-dimensional disturbance amplitudes ($A_{s\beta}$) for (*a*) PH01P, PH$\frac{1}{4}\pi$1P, and PH$\frac{1}{4}\pi$0P (upper three curves at $t = 10$ are A_{s1} and lower three are $A_{s\frac{1}{2}}$) and (*b*) WMID2P ($A_{s\frac{3}{4}}$ not initialized).

Simulation	A_{10} $\times 10^2$	$A_{\frac{1}{2}0}$ $\times 10^2$	$A_{\frac{1}{4}0}$ $\times 10^2$	A_{01}† $\times 10^2$	$A_{0\frac{1}{2}}$† $\times 10^2$	$A_{0\frac{1}{4}}$† $\times 10^2$	$\phi_{0\frac{1}{2}}$	$\phi_{0\frac{1}{4}}$	τ_r	τ_{o0}	τ_{p1}	τ_{s1}	τ_{p2}	τ_{s2}
PH$\frac{1}{4}\pi$0P	4.00	—	—	8.32	6.66	—	$\frac{1}{4}\pi$	—	12.2	15.4	—	—	—	—
PH01P	4.00	3.00	—	8.32	6.66	—	0	—	11.4	—	22.2	27.1	—	—
PH$\frac{1}{4}\pi$1P	4.00	3.00	—	8.32	6.66	—	$\frac{1}{4}\pi$	—	11.4	—	22.0	27.7	—	—
PH$\frac{1}{8}\pi$1P	4.00	3.00	—	8.32	6.66	—	$\frac{1}{8}\pi$	—	11.4	—	22.0	27.4	—	—
WMID2P	$4.52^{\omega G}$	$3.47^{\omega G}$	$5.14^{\omega G}$	3.18	1.02	1.54	0	0	11.8	—	21.1	31	40.1	54
TURB2P	4.00	3.00	3.00	8.32	6.66	10.11	$\frac{1}{8}\pi$	$\frac{7}{16}\pi$	11.3	—	21.0	29.2	47.1	T

† For comparison with cases cited in Rogers & Moser (1992), $\Gamma_x/A_{0\beta} = 4.382$, 5.472 and 7.210 for disturbances with $\beta = 1$, $\frac{1}{2}$ and $\frac{1}{4}$ respectively.

TABLE 2. Parameters of the three-dimensional simulations. Two-dimensional disturbance profiles are eigenfunctions unless superscripted $^{\omega G}$, in which case they are ωG. Three-dimensional disturbance profiles are ωG. $Re_0 = 250$, $\phi_{z0} = 0$, $\lambda_x = 1.16(2\pi)$ and $\lambda_z = 0.6\lambda_x$ for all cases. A 'T' indicates that the flow is too 'turbulent' for τ_{s2} to be well-defined. Numbers given with less precision (τ_s) are the result of $-\omega_h$ not being computed at every time step for WMID2P. All the flows were either too 'turbulent' or not computed long enough to determine τ_{o1} and τ_{o2}.

endpoints of the range of non-redundant phases, then the relevant spatial symmetry is preserved.

Following the reasoning used in §2, the dominant spanwise scale (Λ_z) is defined to be the wavelength λ_z/β ($\beta \neq 0$) associated with the maximum amplitude $A_{s\beta}$. By this definition $\Lambda_z = \lambda_z$ initially for all cases discussed here except for the TURB2P flow (described in detail in MR), in which $\Lambda_z = 4\lambda_z$ at $t = 0$. A scale change is said to occur when Λ_z changes. Since the simulations have a finite spanwise domain not more than four times larger than λ_z, there are only a few discrete wavelengths near λ_z that can be represented. Thus any scale changes that occur, must occur at discrete times. There can be no gradual change in Λ_z. The time τ_{sc} is defined to be the time at which such a scale change occurs. Note that scale change as defined here reflects a change in the energy of spanwise Fourier modes. Such a scale change does not necessarily imply a change from an array of rib vortices at one spacing to similar rib vortices at another spacing (see §3.2).

3.1. *Fourier analysis*

The evolution of A_{s1} and $A_{s\frac{1}{2}}$ for the PH01P, PH$\frac{1}{4}\pi$1P, and PH$\frac{1}{4}\pi$0P simulations (see table 2) is shown in figure 4(*a*). A scale change occurs in each of these cases (even the non-pairing case, PH$\frac{1}{4}\pi$0P) at times τ_{sc} of 31.5, 29.4, and 28.9 respectively. Scale

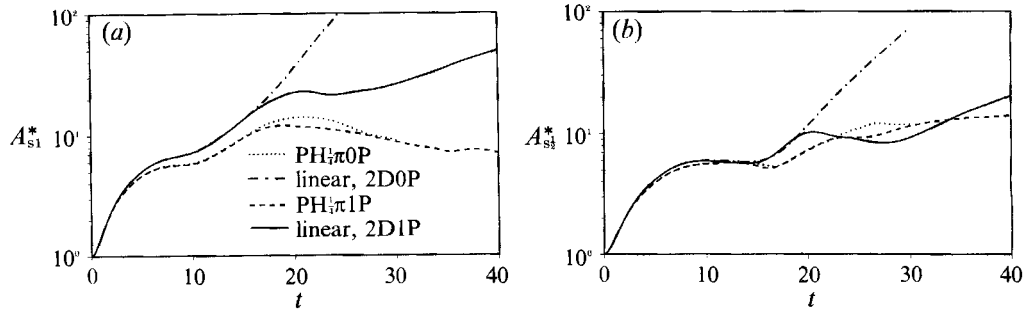

FIGURE 5. Time development of (a) A^*_{s1} and (b) $A^*_{s\frac{1}{2}}$.

change occurs first in the *non-pairing* case because the pairing suppresses the growth of $A_{s\frac{1}{2}}$. In the pairing cases, the two phasings have different scale change times because at $t \approx 20$, the growth of $A_{s\frac{1}{2}}$ is delayed for PH01P. An intermediate phasing case (PH$\frac{1}{8}\pi$1P) was also simulated (not shown in figure 4) and had a scale change time intermediate between PH01P and PH$\frac{1}{4}\pi$1P ($\tau_{sc} = 29.9$).

These scale changes are much more rapid than those in the linear analysis of §2, which implies that the scale change in these cases is essentially nonlinear. In figure 5, A^*_{s1} and $A^*_{s\frac{1}{2}}$ from PH$\frac{1}{4}\pi$1P and PH$\frac{1}{4}\pi$0P are compared with those from the corresponding linear analysis. The most important difference between the linear and nonlinear cases is that the nonlinear $\beta = 1$ modes have saturated, as was observed in MR. That is, A^*_{s1} does not grow beyond $t = 20$ and the growth prior to this is less than that for the linear perturbation. This saturation occurs in the non-pairing case as well, despite the fact that the linear analysis perturbations are undergoing post-oversaturation exponential growth (see MR). In contrast, $A^*_{s\frac{1}{2}}$ does not stop growing, although it does evolve nonlinearly. $A^*_{s\frac{1}{2}}$ even exceeds the linear results at around $t = 30$ in the pairing case. Thus it is the nonlinear saturation of the fundamental ($\beta = 1$) coupled with the continued growth of the subharmonic ($\beta = \frac{1}{2}$) that allows the spanwise scale to change. To confirm this, we examine WMID2P (figure 4*b*). This flow has weaker initial three-dimensional disturbances, which therefore saturate later. The scale change occurs much later in this case (after the second pairing, $\tau_{sc} = 61.0$), and only after A_{s1} has saturated.

3.2. *Spanwise scale change mechanisms*

The most obvious structural manifestations of the three-dimensionality in the mixing layer are the rib vortices that reside in the braid regions. It is therefore expected that any change in the dominant spanwise lengthscale will be accompanied by a reorganization of the rib vortices at the new lengthscale. It is the mechanism for this reorganization that is of interest here. In flows undergoing a nonlinear spanwise scale change, the ribs are collapsed into compact nearly circular vortices as described by Lin & Corcos (1984) because collapse of the ribs is one of the first nonlinear features to develop (Rogers & Moser 1992). To track the evolution of the ribs, the streamwise vorticity in a (z, y)-plane passing through the middle of the braid region (mid-braid plane) will be examined. This plane, located at $x = 0$, is denoted by MP.

To understand how the ribs in the mid-braid plane evolve, we must first examine the physical consequences of the different phasings of the subharmonics. When subharmonic $(0, \beta)$ modes are included, the resulting rib vortices are no longer uniform in strength. The initial patterns of rib strength variation for $\phi_{0\frac{1}{2}}$ of 0 and $\frac{1}{4}\pi$ are shown in figure 6(*a*, *d*). The $\phi_{0\frac{1}{2}} = 0$ phase (PH01P) results in ribs of two

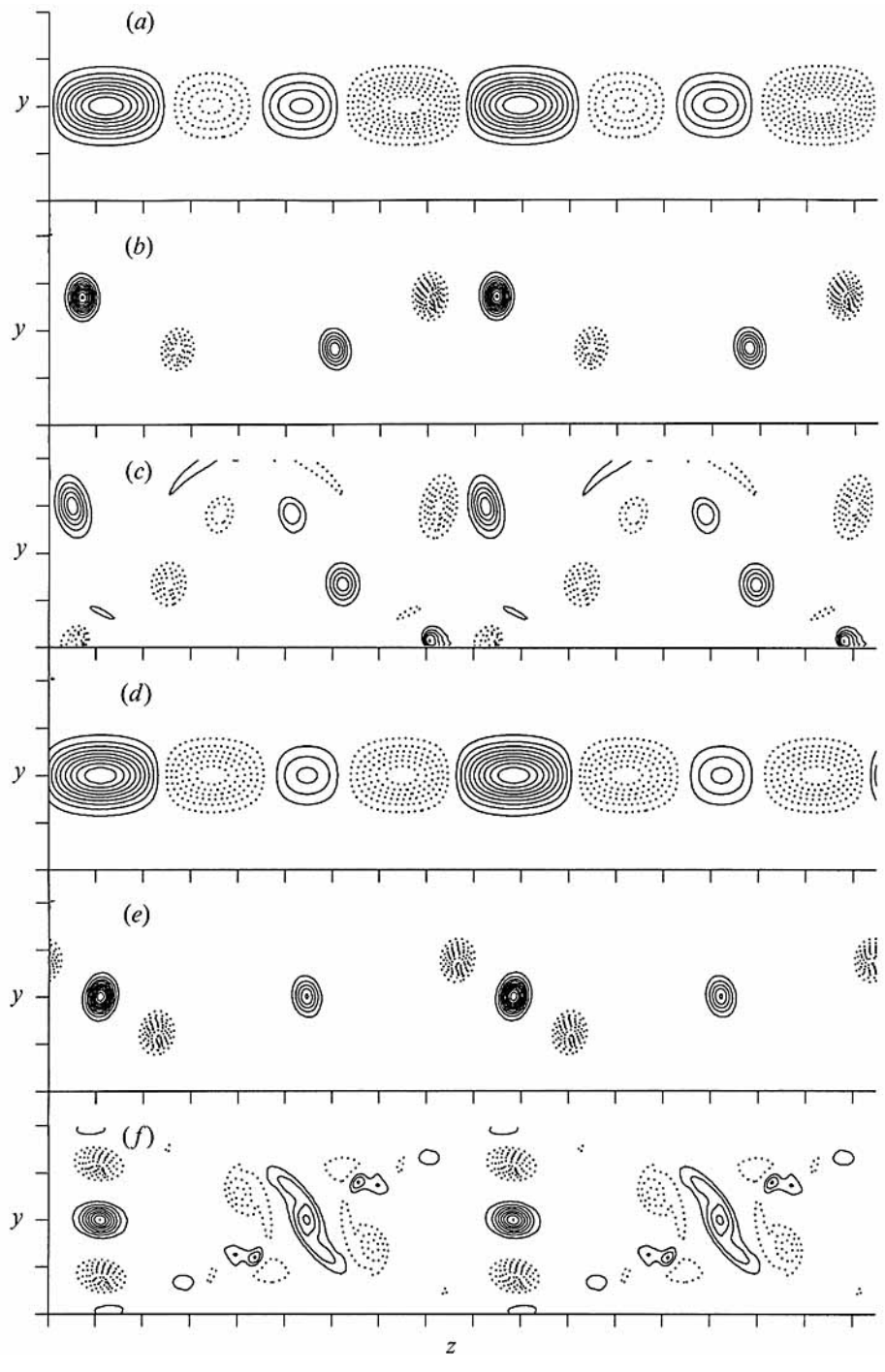

FIGURE 6. Contours of ω_z in the MP for (*a*, *b*, *c*) PH01P and (*d*, *e*, *f*) PH$\frac{1}{4}\pi$1P. Times are (*a*, *d*) 0, (*b*) 27.2 ($\tau_{s1} = 27.1$, $\tau_{sc} = 31.5$), (*c*) 34.6, (*e*) 28.1 ($\tau_{s1} = 27.7$, $\tau_{sc} = 29.4$), (*f*) 34.6. The contour increment is ± 1.0 except for (*a*), (*d*) ($t = 0$) where it is ± 0.04. The spanwise domain has been extended using periodicity to $2L_z = 4\lambda_z$.

strengths, arranged with a strong pair and a weak pair next to each other (figure 6*a*). This preserves the plane-reflection symmetry (MR, equation (10)) as discussed above. The other extreme phasing ($\phi_{0\frac{1}{2}} = \frac{1}{4}\pi$, PH$\frac{1}{4}\pi$1P) produces ribs of three strengths, a strong and weak rib of the same sign and two opposite-signed medium strength ribs (figure 6*d*). With this phasing the point-reflection symmetry (MR, equation (11)) is preserved, with the symmetry points located in the middle of the strongest and weakest ribs. Intermediate phasings result in a rib pattern intermediate between the above extremes, and have no symmetries (PH$\frac{1}{8}\pi$1P).

As the mixing layer evolves, spanwise vorticity is removed from the braid region, and the ribs collapse. Once this has occurred, the evolution of the ribs in the MP is largely determined by the net induced motion of each rib vortex on the rest of the ribs. (Note that an array of uniform-strength ribs do not move from their MP locations at $y = 0$ (see MR).) In PH01P, the strong rib pair drives itself upward (for the sign shown in figure 6*a*) and the weak rib pair moves downward. Once away from the centreline, the weaker ribs drive the strong pair together, while being separated by the induced motion of the stronger ribs (figure 6*b*, *c*). All of the ribs are prevented from moving too far from the centreline by the compressive component of the strain associated with the primary roller vortices. In PH$\frac{1}{4}\pi$1P, the rib motion is dominated by the strongest rib, which remains fixed at the same location due to the point symmetry (as does the weakest rib). The two intermediate-strength ribs rotate around the strongest rib and, because of the induced motion of the weakest rib, slowly spiral inwards (figure 6*e*, *f*). In both flows (figure 6*c*, *f*) these self-induced rib motions continue for some time after τ_{s1} despite the presence of additional vorticity in the MP, which is generated when spanwise vorticity re-enters the braid region at τ_{s1} (see MR). By $t = 35$, the intermediate-strength ribs in PH$\frac{1}{4}\pi$1P (negative ω_x in figure 6*f*) are directly above and below the strongest (positive) rib vortex. At this point, however, many new regions of significant ω_x are present in the mid-braid plane and shortly after this the flow appears 'turbulent', with little evidence of the original rib vortices. As expected, the PH$\frac{1}{8}\pi$1P evolution (see Moser & Rogers 1992) is intermediate between that of the two extreme cases discussed above.

The above rib behaviour suggests two possible mechanisms for a spanwise scale change. The first, associated with $\phi_{0\frac{1}{2}} = 0$, may result from viscous annihilation of a strong vortex pair that is being compressed together, similar to the mechanism proposed by Jimenez (1983). The second, suggested by the $\phi_{0\frac{1}{2}} = \frac{1}{4}\pi$ case, occurs when the inwardly spiralling, intermediate-strength vortices viscously combine with a stronger rib, resulting in a weak rib with the sign of the original intermediate-strength pair. Both of these mechanisms depend on viscosity to be carried to completion, and are therefore slow. In practice, even flows resulting from large $(0, \beta)$ initial disturbances will not complete this process before τ_{s1}, when vorticity re-enters the braid region and greatly increases the complexity of the flow in the braid region. (Weaker initial disturbances that do not result in collapsed ribs show minimal rib movement prior to τ_{s1}). Also both scale change mechanisms result in weak rib pairs with twice the initial spanwise spacing. Thus, if this kind of scale change were carried to completion it would result in a reduction of three-dimensionality (as measured by rib strength). It is instructive to note that the second mechanism (associated with $\phi_{0\frac{1}{2}} = \frac{1}{4}\pi$) results in Fourier mode energies that indicate spanwise scale change long before the complete viscous combination of the three stronger ribs has occurred. In particular, when the intermediate-strength rib pair is situated directly above and below the strongest rib (figure 6*f*), the spanwise variation is primarily accounted for by the $(\alpha, \frac{1}{2})$ modes. In this state $A_{s\frac{1}{2}} > A_{s1}$ (see figure 4*a*). Caution must therefore be

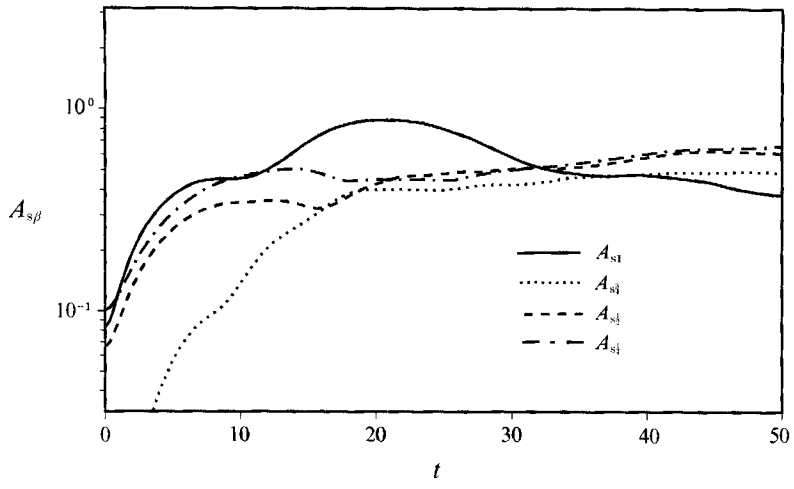

FIGURE 7. Time development of $A_{s\beta}$ ($A_{s\frac{3}{4}}$ not initialized) for TURB2P.

used in drawing conclusions about the structures present in a flow based on the occurrence of the scale change given by Fourier mode energies.

The two scale change mechanisms discussed above occur even in flows that do not possess the spatial symmetries exhibited by PH01P and PH$\frac{1}{4}\pi$1P (e.g. PH$\frac{1}{8}\pi$1P, see Moser & Rogers 1992) and when multiple spanwise subharmonics are present. For example, two spanwise subharmonics were included in the TURB2P case (see table 2), and the subharmonic phases ($\phi_{0\frac{1}{2}} = \frac{1}{8}\pi$ and $\phi_{0\frac{1}{4}} = \frac{7}{16}\pi$) were chosen to get a very irregular initial rib strength distribution with no symmetries. (A second streamwise subharmonic was also included in TURB2P to allow a second pairing, so that the transition to turbulence could be completed (see MR).) A plot of $A_{s\beta}$ for various spanwise wavelengths is shown in figure 7. As can be seen from this figure, a scale change occurs at about the same time as in the previous cases ($\tau_{sc} = 32.0$), but both the $\beta = \frac{1}{2}$ and $\beta = \frac{1}{4}$ modes exceed the fundamental at nearly the same time. (Note that there are three prior crossings of A_{s1} and $A_{s\frac{1}{4}}$ due to the large initial amplitude of $A_{s\frac{1}{4}}$.) Contours of the streamwise vorticity in the surviving MP ($x = 0$) at this time are shown in figure 8. The rib vortices have moved by mutual induction as discussed above and it appears that both scale change mechanisms are occurring at the same time. Shortly after this time, this flow becomes turbulent and it is no longer possible to identify organized rib vortices in the MP. This turbulent flow is discussed in detail in MR.

As noted above, the flow evolution in the MP becomes more complicated when vorticity re-enters this plane at τ_{s1} (or at τ_{o0} in the absence of pairing). Although it appears that the re-entry of spanwise vorticity did not play an important role in the scale changes discussed above, the restructuring of the mid-braid vorticity after τ_{s1} could provide an additional mechanism for changing the characteristic spanwise scale. However, many of the flows examined in the preceding sections become 'turbulent' after τ_{s1}, so that clearly defined ribs are not present to visually determine the spanwise scale (although Λ_z is still well-defined).

To study the impact that re-entry of vorticity into the braid region could have on scale change we again consider WMID2P, a flow with weaker initial perturbations. Figure 9 shows MP contours of ω_x at six different times during the evolution of WMID2P. Just after $\tau_{s1} = 32$ (figure 9*a*), additional streamwise vorticity is visible

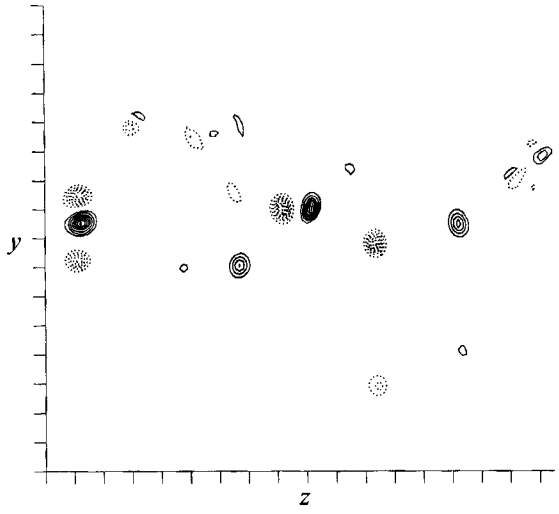

FIGURE 8. Contours of ω_x in the surviving MP of the TURB2P simulation at $t = 32.2$ ($\tau_{s1} = 29.2$, $\tau_{sc} = 32.0$). The contour increment is ± 1.0.

away from the centreline. This vorticity becomes stronger by $\tau_{p2} = 40.1$ (figure 9*b*) and then (because it has the same sign as the rib vorticity at the same spanwise location) 'recollapses' into the ribs, resulting in stronger rib vortices, which are again compact and near the centreline (figure 9*c*). After $\tau_{s2} = 54$ (figure 9*d*) another re-entry of vorticity into the MP occurs. This time, however, ω_x of both signs is generated above and below many of the ribs. The recollapse is thus more complicated (figure 9*f*). Since there is a marked subharmonic component to the re-entering vorticity, it can change the relative strengths of the ribs. At $t = 61.3 \approx \tau_{sc}$ (figure 9*e*) the first mechanism described above (associated with $\phi_{0\frac{1}{2}} = 0$) is active, as evidenced by the two pairs of rib vortices that are compressed together and dropping below the centreline (one on the domain boundary). Indeed eleven time units later (figure 9*f*), there appear to be only two pairs of significant rib vortices, approximately equally spaced and slightly above the centreline. Viscous effects have weakened the remaining ribs whose remnants are still visible in figure 9(*f*). Although the actual scale change in the WMID2P flow occurred by the same mechanism as in PH01P, the recollapse of new vorticity generated by the spiral-arm re-entry may be responsible for speeding up the process by enhancing the non-uniformity of the ribs.

It is perhaps surprising that scale change (as defined here) occurs even in the absence of pairing (see §3.1). This scale change is not predicted by linear analysis (see figure 1*a*). At early times (before $\tau_{00} = 15.4$), the PH$\frac{1}{4}\pi$0P flow evolves like PH$\frac{1}{4}\pi$1P, since the initial three-dimensional perturbations are identical (see figure 4*a*). By $t = 30$ (well beyond τ_{00}) the flow has been 'oversaturated' for a long time and much vorticity has re-entered the braid region, greatly increasing the complexity of the flow (see figure 10). Because of this, the flow appears 'turbulent'. Despite the fact that there are no well-defined ribs, it is clear that a single large-scale structure ($\beta = \frac{1}{2}$) dominates the MP. This scale change is apparently unrelated to the two scale change mechanisms discussed above.†

† Despite the fact that $A_{s\frac{1}{2}} > A_{s1}$ after $\tau_{sc} = 28.9$, $A_{0\frac{1}{2}}$ remains significantly smaller than A_{01}. Thus streamwise-averaged measures of scale change, such as that used by Huang & Ho (1990), would probably not indicate any scale change in this flow.

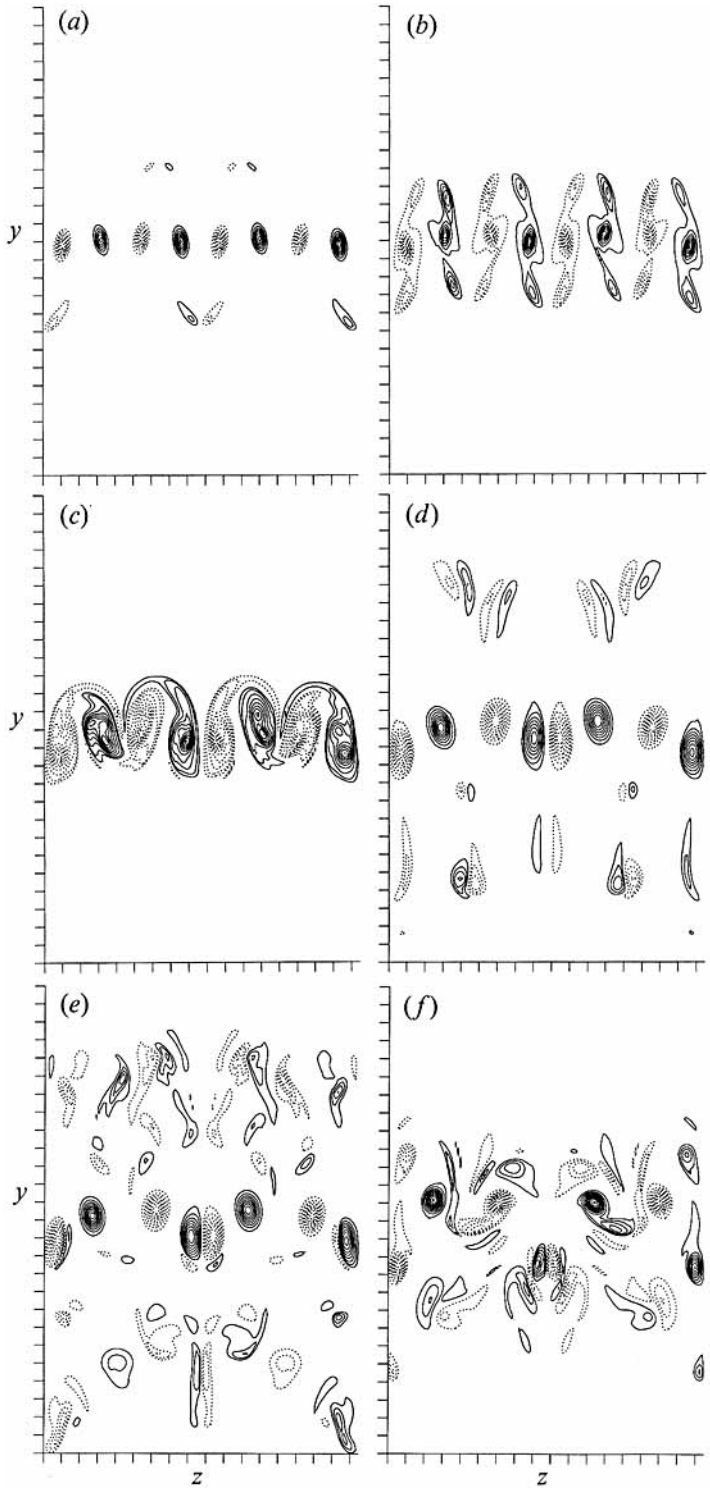

FIGURE 9. Contours of ω_x in the MP of WMID2P at (*a*) $t = 33.6$ ($\tau_s = 31$), (*b*) $t = 40.1 = \tau_{p2}$, (*c*) $t = 46.4$, (*d*) $t = 55.7$ ($\tau_{s2} = 54$), (*e*) $t = 61.3$ ($\tau_{sc} = 61.0$), and (*f*) $t = 72.6$. The contour increments are (*a*, *b*, *c*) ± 0.2, (*d*) ± 0.3, (*e*) ± 0.35, and (*f*) ± 0.4. In (*c*) there is an extra contour at ± 0.1 to show the vorticity crossing over neighbouring ribs.

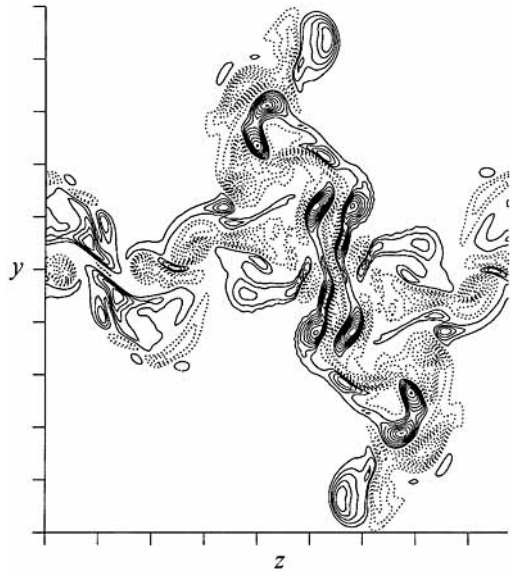

FIGURE 10. Contours of ω_x in the MP of PH$\frac{1}{4}\pi$0P at $t = 30.0$. The contour increment is ± 0.6.

4. Summary and discussion

The work presented here was undertaken to explain the differences between observations (e.g. Bernal & Roshko 1986) that the dominant spanwise lengthscale in a mixing layer remains constant until the mixing (or turbulence) transition and other observations (e.g. Huang & Ho 1990) that the spanwise scale doubles with each pairing. The mechanisms by which such a scale change might occur are also of interest.

Huang & Ho (1990) argue that their experimental observations are consistent with the linear analysis of Pierrehumbert & Widnall (1982), which suggests that there is a preferred spanwise wavelength proportional to the roller spacing in the mixing layer. However, the more detailed linear analysis presented here indicates that the linear mechanism for spanwise scale change is exceptionally slow. Apparently about two pairings are required to double the spanwise wavelength of the fastest growing mode, and as many as four pairings may be required to actually change the dominant (highest energy) spanwise lengthscale. Thus the linear analysis does not support Huang & Ho's picture of self-similar growth of streamwise and spanwise lengthscales. One of the reasons for the slowness of the linear scale change is that the two-dimensional base flow itself is not similar from pairing to pairing. As pointed out in MR and §2, the diameter of the concentrated core of spanwise vorticity in a pairing mixing layer at moderate or high Reynolds number only grows by a factor of $\sqrt{2}$ with each pairing. A scaling in which the spanwise wavelength of the fastest growing mode is proportional to the size of this concentrated vortex core is thus consistent with the results in §2. Also the growth rate of disturbances is not very sensitive to wavelength (for wavelengths near the fastest growing one). Therefore, once a disturbance has become the fastest growing one, a long time is required for it to become the most energetic.

A change in the most energetic spanwise wavelength can occur more rapidly with finite-amplitude (nonlinear) perturbations. Such a scale change can occur after the first pairing, or even in the absence of pairing. Among other things, nonlinearity

stops the growth of the fundamental spanwise disturbance, while allowing longer wavelength disturbances to continue to grow. Depending on the amplitudes of the initial three-dimensional disturbances, a doubling in dominant spanwise scale has been observed to occur after zero, one, or two pairings, and the dominant scale can double or quadruple after one pairing. While a doubling of the most energetic spanwise scale could occur after each of several pairings as suggested by Huang & Ho (1990), such an occurrence would necessarily depend on the details of the disturbance environment and therefore cannot be considered to be a general result.

The definition of dominant spanwise scale used here is based on the amplitude of Fourier modes with a given spanwise wavelength ($A_{s\beta}$). The amplitude of the spanwise Fourier modes with no streamwise variation $A_{0\beta}$ could also have been used. This definition more closely mimics the scale change diagnostic of Huang & Ho (1990) and Bell & Mehta (1992) who examined the time-averaged streamwise velocity as a function of z. Using this scale change measure, scale changes occur later than by the previous definition. For example, in TURB2P the spanwise scale would double at $t = 49.1$ rather than quadruple at $\tau_{sc} = 32.0$. These differences in the scale change diagnostic do not affect our qualitative conclusions regarding the occurrence of scale changes.

By defining scale change in reference to the dominant Fourier mode, there are no implications regarding changes occurring in the flow structures. However, in most discussions of scale change, it is implicitly assumed that the scale change involves a reorganization of the rib vortices into an array of counter-rotating vortices at a new lengthscale. Two mechanisms by which such a reorganization could occur have been identified. First, a strong, roughly equal-strength rib pair will move away from the centreline in the braid, be brought together by the induced motion of neighbouring ribs, and eventually be viscously annihilated (similar to the mechanism proposed by Jimenez 1983). Second, a single strong rib can induce nearby weaker ribs of opposite sign to rotate around it, eventually leading to a viscous amalgamation and a single weaker rib vortex. In addition, these scale change mechanisms may be aided by the re-entry of spanwise vorticity into the braid region, which can enhance the non-uniformity in the strength of the ribs. In both mechanisms, weaker ribs at double the spanwise lengthscale would result if the process were carried to completion. However, completion is by viscous diffusion and is therefore slow. Note that the scale change time, as measured by the Fourier amplitudes, occurs early in the process, long before the actual viscous annihilation or recombination is completed.

In all cases, the scale change mechanisms described above could not proceed to completion. After the process was initiated, and the dominant scale changed (according to the Fourier mode definitions given above), highly three-dimensional vorticity associated with the transition to turbulence entered the braid region, making it difficult to identify the rib vortices. Apparently rib vortices that are strong enough to initiate the nonlinear scale change (they must at least be collapsed in the sense of Lin & Corcos 1984) are also strong enough to initiate the transition to turbulence as discussed in MR. The simple scenario of an array of rib vortices being transformed into a similar array with a new, larger lengthscale does not occur. Spanwise scale change occurs only in the statistical sense of an increase in the wavelength of the dominant Fourier mode.

In conclusion, the main reason for the apparent difference between observations that a scale change occurs after each pairing (Huang & Ho 1990) and observations that scale changes do not occur until the transition (e.g. Bernal & Roshko 1986) is probably the difference in disturbance environments in the experimental facilities.

The data upon which Huang & Ho (1990) based their conclusion that the spanwise scale doubles with each pairing are the result of a particular disturbance environment that produced this result for the first two pairings. Initial disturbance levels could certainly be chosen that reproduce this behaviour in a numerical simulation. It is also important to remember that when the three-dimensional disturbances are strong enough to produce a rapid scale change (as in the experiments mentioned above), then the scale change is accompanied by the onset of the transition to turbulence. This is consistent with the results of both Huang & Ho (transition starts at about the first pairing) and Bernal & Roshko, as well as other experiments (e.g. Jimenez 1983). Thus, a simple array of counter-rotating rib vortices at the new spanwise scale does not exist after a scale change.

This work was initiated to answer questions posed by Professor C.-M. Ho during the 1988 Center for Turbulence Research Summer School Program and we are grateful for his inspiration. Helpful comments provided by Dr N. Mansour and Professor S. K. Lele on a draft of this paper are also appreciated. Some of the computations were performed on the NAS supercomputers at NASA Ames Research Center.

REFERENCES

BELL, J. H. & MEHTA, R. D. 1992 Measurements of the streamwise vortical structures in a plane mixing layer. *J. Fluid Mech.* **239**, 213–248.

BERNAL, L. P. 1981 The coherent structure of turbulent mixing layers. Ph.D. thesis, California Institute of Technology.

BERNAL, L. P. & ROSHKO, A. 1986 Streamwise vortex structure in plane mixing layers. *J. Fluid Mech.* **170**, 499–525.

BREIDENTHAL, R. 1981 Structure in turbulent mixing layers and wakes using a chemical reaction. *J. Fluid Mech.* **109**, 1–24.

BROWN, G. L. & ROSHKO, A. 1974 On density effects and large structure in turbulent mixing layers. *J. Fluid Mech.* **64**, 775–816.

CORCOS, G. M. & LIN, S. J. 1984 The mixing layer: deterministic models of a turbulent flow. Part 2. The origin of the three-dimensional motion. *J. Fluid Mech.* **139**, 67–95.

HUANG, L.-S. & HO, C.-M. 1990 Small-scale transition in a plane mixing layer. *J. Fluid Mech.* **210**, 475–500.

JIMENEZ, J. 1983 A spanwise structure in the plane shear layer. *J. Fluid Mech.* **132**, 319–336.

JIMENEZ, J., COGOLLOS, M., BERNAL, L. P. 1985 A perspective view of the plane mixing layer. *J. Fluid Mech.* **152**, 125–143.

KONRAD, J. H. 1976 An experimental investigation of mixing in two-dimensional turbulent shear flows with applications to diffusion-limited chemical reactions. *Internal Rep.* CIT-8-PU. Calif. Inst. Technol. Pasadena, CA.

LASHERAS, J. C., CHO, J. S. & MAXWORTHY, T. 1986 On the origin and evolution of streamwise vortical structures in a plane, free shear layer. *J. Fluid Mech.* **172**, 231–258.

LASHERAS, J. C. & CHOI, H. 1988 Three-dimensional instability of a plane free shear layer: an experimental study of the formation and evolution of streamwise vortices. *J. Fluid Mech.* **189**, 53–86.

LIN, S. J. & CORCOS, G. M. 1984 The mixing layer: deterministic models of a turbulent flow. Part 3. The effect of plane strain on the dynamics of streamwise vortices. *J. Fluid Mech.* **141**, 139–178.

MIKSAD, R. W. 1972 Experiments on the nonlinear stages of free-shear-layer transition. *J. Fluid Mech.* **56**, 695–719.

MOSER, R. D. & ROGERS, M. M. 1992 The three-dimensional evolution of a plane mixing layer Part 2: Pairing and transition to turbulence. *NASA TM*103926.

MOSER, R. D. & ROGERS, M. M. 1993 The three-dimensional evolution of a plane mixing layer: pairing and transition to turbulence. *J. Fluid Mech.* **247**, 275–320 (referred to herein as MR).

NYGAARD, K. J. & GLEZER, A. 1991 Evolution of streamwise vortices and generation of small-scale motion in a plane mixing layer. *J. Fluid Mech.* **231**, 257–301.

PIERREHUMBERT, R. T. & WIDNALL, S. E. 1982 The two- and three-dimensional instabilities of a spatially periodic shear layer. *J. Fluid Mech.* **114**, 59–82.

ROGERS, M. M. & MOSER, R. D. 1992 The three-dimensional evolution of a plane mixing layer: the Kelvin–Helmholtz rollup. *J. Fluid Mech.* **243**, 183–226.

SPALART, P. R., MOSER, R. D. & ROGERS, M. M. 1991 Spectral methods for the Navier-Stokes equations with one infinite and two periodic directions. *J. Comput. Phys.* **96**, 297–324.

STUART, J. T. 1967 On finite amplitude oscillations in laminar mixing layers. *J. Fluid Mech.* **29**, 417–440.

WALEFFE, F. 1990 On the three-dimensional instability of strained vortices. *Phys. Fluids* A **2**, 76–80.